Shear-Induced Phase Separation in Solutions of Wormlike Micelles

Beth A. Schubert, Norman J. Wagner, and Eric W. Kaler

Department of Chemical Engineering, University of Delaware, Newark, Delaware 19716

Srinivasa R. Raghavan*

Department of Chemical Engineering, University of Maryland, College Park, Maryland 20742-2111

Received September 27, 2003. In Final Form: December 5, 2003

Polymer solutions in the vicinity of the θ-point are known to undergo shear-induced turbidity or phase separation. The present study shows that a similar phenomenon also occurs for certain wormlike micellar solutions. Wormlike micelles are the self-assembled counterparts of polymers and are characterized by their ability to reversibly break and recombine. In the system of interest, the micelles are formed by the cationic surfactant erucyl bis(hydroxyethyl)methylammonium chloride (EHAC), in conjunction with a salt such as sodium chloride (NaCl) or sodium salicylate (NaSal). Micellar samples that become turbid under shear show evidence of critical concentration fluctuations and may contain predominantly branched micelles. The shear-induced turbidity in these samples correlates with the appearance of flow-dichroism in rheo-optic experiments and with an increase in low-q scattering in small-angle light scattering under flow (flow-SALS) experiments. The characteristic "butterfly" pattern, with enhanced scattering in the flow direction and a dark streak perpendicular to the flow direction, is typically observed in flow-SALS. The results suggest that the turbidity is due to a shear-induced growth of concentration fluctuations, which in turn manifests as large anisotropic domains, typically oriented along the vorticity axis.

Introduction

Under the appropriate conditions (temperature, salt and surfactant concentration, etc.), surfactant molecules can self-assemble into long, flexible chains referred to as wormlike or threadlike micelles.[1−3] Similar to polymers, these chains also form entangled networks in semidilute solutions, giving rise to highly viscoelastic fluids. Unlike most polymers, however, wormlike micelles break and re-form dynamically. If this process is sufficiently rapid, the solution viscoelasticity is well-approximated by a Maxwell fluid with a single relaxation time.[2] The analogy between wormlike micelles and polymers is a subject of lively debate, and many similarities in the rheology and dynamics of the two systems have been noted (e.g., the plateau modulus G_p increases with concentration as $\sim c^{2.2}$ for both cases).[2] In this paper, we show that some wormlike micellar solutions also tend to exhibit *shear-induced phase separation*, a nonequilibrium phenomenon that has been predominantly associated with polymer solutions.

Shear-induced phase separation (SIPS) has been reported for semidilute solutions of some polymers in marginal or theta-solvents.[4−10] These solutions turn visibly turbid when sufficient shear is imposed, and upon shear cessation the solutions revert to their clear state. The turbidity has been shown to arise from a shear-induced enhancement of polymer concentration fluctuations.[5] Thus, the phenomenon is not a true thermodynamic phase transition but a nonequilibrium result of the coupling between hydrodynamic stress and concentration in a polymeric fluid. In light or neutron scattering experiments on a fluid under shear, the concentration fluctuations give rise to an anisotropic "butterfly pattern", where the scattering is enhanced in the direction of the flow and depressed in the direction perpendicular to the flow.[8−10] Indeed, the butterfly pattern indicates the hydrodynamic origin of this effect.

Shear-induced turbidity in polymer solutions has been investigated using rheo-optics by several groups.[6,7] At the onset of turbidity, the sample exhibits a negative flow-dichroism due to scattering from micron-sized, elongated domains. These domains correspond to shear-enhanced concentration fluctuations and are often oriented perpendicular to the flow-gradient plane along the vorticity axis.[6] With further increases in shear rate, the dichroism may reverse sign from negative to positive, suggesting that the domains orient along the streamlines.[11−13] It is significant that flow-dichroism does not develop in solutions that remain clear under shear. On the other hand, both clear and turbid polymer solutions exhibit flow-birefringence, and its magnitude increases monotonically with shear rate.[7] Thus, flow-birefringence reflects the segmental alignment of flexible-chain polymers under shear, while dichroism tracks the growth of anisotropic concentration fluctuations.

* Corresponding author. E-mail: sraghava@eng.umd.edu.

(1) Rehage, H.; Hoffmann, H. *Mol. Phys.* **1991**, *74*, 933.
(2) Cates, M. E. *J. Phys. Chem.* **1990**, *94*, 371.
(3) Cates, M. E. *J. Phys.: Condens. Matter* **1996**, *8*, 9167.
(4) Onuki, A. *J. Phys.: Condens. Matter* **1997**, *9*, 6119.
(5) Helfand, E.; Fredrickson, G. H. *Phys. Rev. Lett.* **1989**, *62*, 2468.
(6) Yanase, H.; Moldenaers, P.; Mewis, J.; Abetz, V.; Vanegmond, J.; Fuller, G. G. *Rheol. Acta* **1991**, *30*, 89.
(7) McHugh, A. J.; Immaneni, A.; Edwards, B. J. In *Flow-Induced Structure in Polymers*; American Chemical Society: Washington, DC, 1995; Vol. 597, p 75.
(8) Moses, E.; Kume, T.; Hashimoto, T. *Phys. Rev. Lett.* **1994**, *72*, 2037.
(9) Migler, K.; Liu, C. H.; Pine, D. J. *Macromolecules* **1996**, *29*, 1422.
(10) Morfin, I.; Lindner, P.; Boue, P. *Macromolecules* **1999**, *32*, 7208.
(11) Kume, T.; Hashimoto, T.; Takahashi, T.; Fuller, G. B. *Macromolecules* **1997**, *30*, 7232.
(12) Minale, M.; Wissbrun, K. F.; Massouda, D. F. *J. Rheol.* **2003**, *47*, 1.
(13) Saito, S.; Koizumi, S.; Matsuzaka, K.; Suehiro, S.; Hashimoto, T. *Macromolecules* **2000**, *33*, 2153.

10.1021/la035810d CCC: $27.50
Published on Web 03/30/2004

Recently, shear-induced turbidity has also been observed in other kinds of complex fluids. Le Mains and Tassin[14] reported this phenomenon for aqueous solutions of telechelic associative polymers (bearing C18 hydrophobes at the ends of the polymer chain). Krishnan et al.[15] observed shear-induced turbidity in polymeric bicontinuous microemulsions consisting of two homopolymers and a diblock copolymer. Remarkably, both these classes of fluids showed a plateau in the shear stress as a function of shear rate, a feature also exhibited by wormlike micellar solutions.

Concerning wormlike micellar fluids, a variety of shear-induced phenomena have been reported.[16−26] The term "shear-induced phase transition" is often encountered, but it usually refers to a different physical phenomenon.[26] For instance, several authors have interpreted the stress plateau found in the rheology of wormlike micellar fluids as evidence for a flow-induced phase transition.[3,17,18] This plateau corresponds either to the formation of a shear-banded flow[17] (where fluid layers of different viscosity coexist) or to a shear-induced transition from an isotropic to a nematic phase.[18] Others have attributed the shear-thickening shown by dilute wormlike micellar fluids to the shear-induced formation of a "gel" phase.[19,20] However, neither the stress plateau nor shear thickening are necessarily accompanied by an increase in the solution turbidity.

There do exist a few reports of shear-induced turbidity in wormlike micellar fluids.[18−25] Pine and co-workers[19,20] found that a solution containing equimolar amounts of the surfactant tris(2-hydroxyethyl) tallowalkylammonium acetate and the salt sodium salicylate separated into two coexisting phases when sheared at constant stress (but not when sheared at constant rate). Fischer and co-workers[21,22] observed a series of alternating turbid and clear rings in the shear-thickening regime of an equimolar cetylpyridinium chloride/sodium salicylate solution. Although these observations are noteworthy, a coherent picture of shear-induced turbidity in wormlike micellar fluids has yet to emerge and important questions remain to be answered. For example, do all wormlike micellar solutions phase-separate under shear, or only those at certain locations on the phase diagram? Further, are the physical manifestations of the shear-induced transitions in wormlike micellar solutions similar to or distinct from the corresponding observations for polymer solutions? To answer these questions, an understanding of the shear-induced phase behavior in the context of the equilibrium phase behavior and microstructure is necessary.

In previous work, we have characterized the rheology, phase behavior, and equilibrium microstructure of a new wormlike micellar system based on a C_{22}-tailed cationic surfactant and salt.[27,28] The corresponding fluids are distinguished both by their unusually pronounced viscoelasticity (solution viscosities orders of magnitude higher than that for comparable systems) and by the rich diversity of their equilibrium phase behavior. Depending on the type and concentration of salt, there are both upper and lower consolute phase boundaries in these systems.[28] In this paper, we report that, depending on their location on the equilibrium phase diagram, some of these solutions exhibit shear-induced phase separation.

Experimental Section

Materials. The surfactant erucyl bis(hydroxyethyl)methylammonium chloride (EHAC), $C_8H_{17}-CH=CH-C_{12}H_{24}-N(C_2H_4OH)_2CH_3$, was a commercial product manufactured by Akzo Nobel, Chicago, IL. Sodium chloride and sodium salicylate (*o*-hydroxy benzoate) were of >99% purity (Aldrich). Solutions containing surfactant and salt were prepared using Nanopure deionized water. The phase behavior of these mixtures has been reported previously.[28]

Rheology. Rheological experiments at 25 °C were performed on a Bohlin CS-50 stress-controlled rheometer and on a Rheometric Scientific ARES strain-controlled rheometer. A cone-and-plate geometry (cone of 50 mm diameter and 0.04 rad angle) was used with both instruments. Rheological studies on these samples have been discussed in detail in previous publications.[27,28]

Rheo-Optics. Rheo-optic experiments were performed using the Optical Analysis Module (OAM) on a Rheometric Scientific ARES rheometer. The sample was placed in a couette cell having an inner bob of 30 mm diameter and an annulus of 2 mm. The temperature was maintained at 25 °C by a forced-air oven. Linearly polarized light from a He−Ne laser ($\lambda = 632.8$ nm) was passed through the sample parallel to the axis of rotation (Figure 1a), thereby enabling rheo-optic studies in the flow-gradient plane. The optical path length was 20 mm. Analysis of the transmitted light yielded the quantities of interest, viz., the birefringence ($\Delta n'$), the dichroism ($\Delta n''$), and the transmitted light intensity (I_{DC}). The transmitted intensity was normalized by the I_{DC} value at rest to give the normalized transmittance T^*, which takes on values from 1 (clear sample) to 0 (completely turbid sample).

Small-Angle Light Scattering under Flow (Flow-SALS). Static light scattering measurements under shear were performed using the optical train of a Rheometrics Optical Analyzer (ROA) modified to project the two-dimensional scattering pattern directly onto the optical chip of a CCD camera. A He−Ne laser ($\lambda = 632.8$ nm) was used to enable an accessible range of scattering vectors q from 0.0018 to 0.008 Å^{-1}. The accuracy of the scattering vector (q) scale was checked by comparing the scattering curve of 2.8 μm polystyrene latex spheres (Interfacial Dynamics) with that from Lorenz−Mie theory.[29,30]

The sample was placed in a 0.28-mm-gap parallel plate geometry thermostated by a fluid bath to 25 °C. The laser was sent through the sample parallel to the flow-gradient direction (Figure 1b), thereby enabling two-dimensional scattering patterns to be collected in the flow-vorticity plane. The scattering patterns were stored as MPEG movie files at a rate of 30 frames per second. To ensure that a steady-state pattern was obtained at each shear rate, the time of each shear zone was chosen based on the transient rheological and rheo-optical behavior of each sample. The final scattering pattern was obtained by averaging frames collected during the final 30 s of shear after steady state was achieved.

Sector averages over 15° were calculated in the flow (x-axis) and vorticity (z-axis) directions. Following the methods of Hashimoto,[11,31] the intensities along the flow and vorticity directions were integrated and normalized by their at-rest value

(14) Le Meins, J. F.; Tassin, J. F. *Macromolecules* **2001**, *34*, 2641.
(15) Krishnan, K.; Chapman, B.; Bates, F. S.; Lodge, T. P.; Almdal, K.; Burghardt, W. R. *J. Rheol.* **2002**, *46*, 529.
(16) Rehage, H.; Hoffmann, H. *Rheol. Acta* **1982**, *21*, 561.
(17) Cappelaere, E.; Berret, J. F.; Decruppe, J. P.; Cressely, R.; Lindner, P. *Phys. Rev. E* **1997**, *56*, 1869.
(18) Decruppe, J. P.; Lerouge, S.; Berret, J. F. *Phys. Rev. E* **2001**, *6302*, 2501.
(19) Hu, Y. T.; Boltenhagen, P.; Pine, D. J. *J. Rheol.* **1998**, *42*, 1185.
(20) Boltenhagen, P.; Hu, Y. T.; Matthys, E. F.; Pine, D. J. *Phys. Rev. Lett.* **1997**, *79*, 2359.
(21) Wheeler, E. K.; Fischer, P.; Fuller, G. G. *J. Non-Newtonian Fluid Mech.* **1998**, *75*, 193.
(22) Fischer, P.; Wheeler, E. K.; Fuller, G. G. *Rheol. Acta* **2002**, *41*, 35.
(23) Fujii, S.; Isojima, T.; Hamano, K. *Phys. Lett. A* **1999**, *263*, 393.
(24) Lu, B.; Li, X.; Scriven, L. E.; Davis, H. T.; Talmon, Y.; Zakin, J. *Langmuir* **1998**, *14*, 8.
(25) Nowak, M. *Rheol. Acta* **1998**, *37*, 336.
(26) Olmsted, P. D. *Curr. Opin. Colloid Interface Sci.* **1999**, *4*, 95.
(27) Raghavan, S. R.; Kaler, E. W. *Langmuir* **2001**, *17*, 300.
(28) Raghavan, S. R.; Edlund, H.; Kaler, E. W. *Langmuir* **2002**, *18*, 1056.
(29) Mie, G. *Ann. Phys.* **1908**, *25*, 377.
(30) Lorenz, L. *Det Kongelige Danske Videnskabernes Selskabs Skrifter* **1890**, *6*, 1.
(31) Saito, S.; Hashimoto, T. *J. Chem. Phys.* **2001**, *114*, 10531.

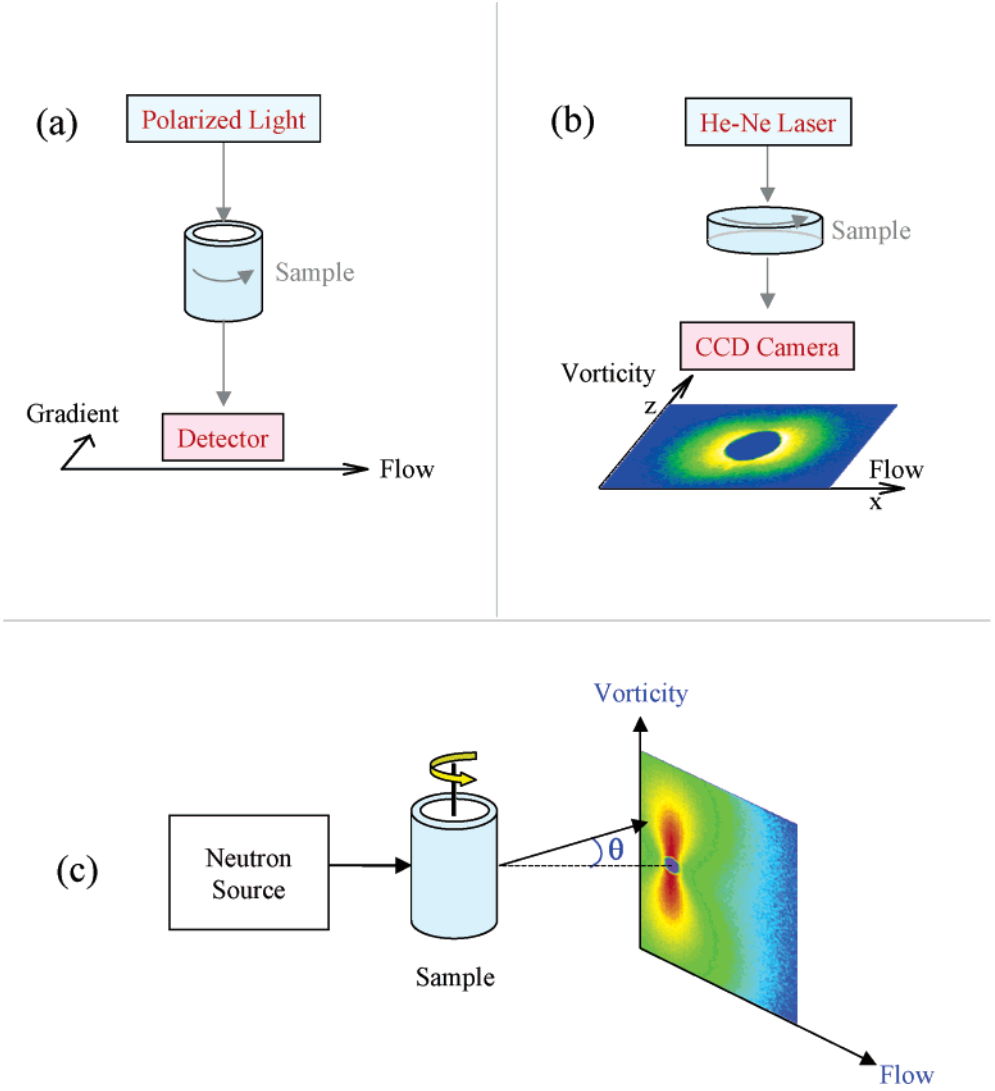

Figure 1. Schematic of (a) rheo-optic experiments, (b) flow-SALS experiments, and (c) flow-SANS experiments.

to provide a method of quantifying the critical shear rate from the data:

$$\mathcal{J}_x(\dot{\gamma}) = \int_{q_{x,\min}}^{q_{x,\max}} I(q_x;\dot{\gamma})\, dq_x / \int_{q_{x,\min}}^{q_{x,\max}} I(q_x;\dot{\gamma}=0)\, dq_x \qquad (1)$$

$$\mathcal{J}_z(\dot{\gamma}) = \int_{q_{z,\min}}^{q_{z,\max}} I(q_z;\dot{\gamma})\, dq_z / \int_{q_{z,\min}}^{q_{z,\max}} I(q_z;\dot{\gamma}=0)\, dq_z \qquad (2)$$

where $I(q_x, \dot{\gamma})$and $I(q_z, \dot{\gamma})$ are the 15° sectoral averages of the intensity in the flow and vorticity directions at a given shear rate $\dot{\gamma}$, and $q_{x,\min}$, $q_{x,\max}$, $q_{z,\min}$, and $q_{z,\max}$ define the limits of the experimental q-range.

Small-Angle Neutron Scattering under Flow (Flow-SANS). Flow-SANS experiments were conducted at NIST, Gaithersburg, MD. The sample was placed in a quartz couette cell with an outer rotating cylinder of radius 29.5 mm and an annulus of 0.5 mm. A neutron beam of wavelength $\lambda = 6$ Å was incident perpendicular to the flow direction (Figure 1c), and the two-dimensional scattering pattern was collected in the flow-vorticity plane. The scattering spectra were corrected for background, empty cell scattering, and transmission and placed on an absolute scale using calibration standards. All experiments were done at 25 ± 0.1 °C. SANS spectra under shear were anisotropic, and intensity averages of these spectra were obtained over 15° sectors about the flow and vorticity directions. The data are shown in terms of the absolute scattered intensity I as a function of the scattering vector $q = (4\pi/\lambda)\sin(\theta/2)$ where λ is the wavelength of incident neutrons and θ is the scattering angle. To quantify the anisotropy observed in the SANS patterns, an alignment factor, defined by

$$A_f = (I_{90} - I_0)/I_{90} \qquad (3)$$

is calculated for each shear rate. Here I_0 and I_{90} are 15° sectoral averages of the intensity in the flow (azimuthal angle $\phi = 0°$) and vorticity ($\phi = 90°$) directions, respectively, and the alignment factor is averaged over the q-range 0.02−0.04 Å^{-1}. At rest, when there is no alignment, $A_f = 0$, and when the micelles are perfectly aligned, $A_f = 1$.

Results

A. EHAC/NaCl Micellar Solutions. It is useful to first recapitulate the phase behavior and rheology of EHAC/NaCl mixtures.[27,28] The phase diagram for 40 mM EHAC solutions as a function of temperature is reproduced in Figure 2a. For salt concentrations (c_{NaCl}) exceeding 1200 mM, the solutions separate into two liquid phases with a distinct meniscus between the phases. The solutions also phase-separate when cooled below the coexistence curve, but in this case, the two-phase samples remain as turbid dispersions. The corresponding rheology of EHAC/NaCl solutions at 25 °C is reproduced in Figure 2b. The zero-shear viscosity η_0 goes through a maximum as a function of c_{NaCl}. Samples near the viscosity maximum are in fact gels; that is, they do not show a plateau in viscosity at low shear rates.[27] The viscosity values shown

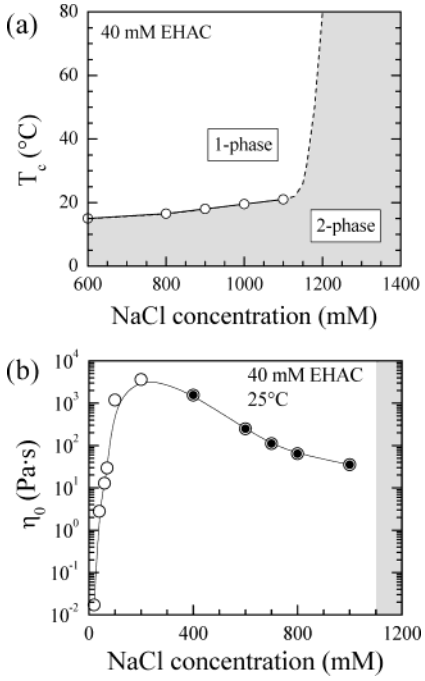

Figure 2. Phase behavior and rheology of EHAC/NaCl mixtures at a fixed EHAC content of 40 mM (ref 28): (a) coexistence temperature T_c vs salt concentration; (b) zero-shear viscosity η_0 at 25 °C vs salt concentration. The filled circles in panel b denote samples that show shear-induced turbidity.

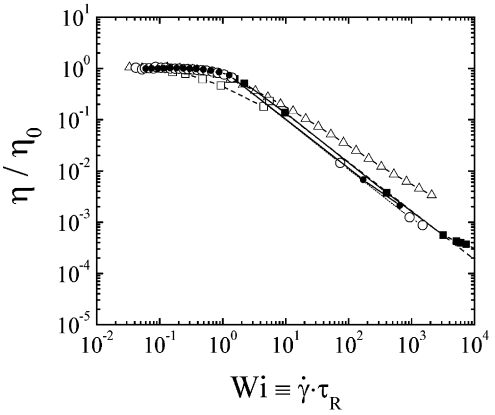

Figure 3. Steady-shear rheology for 40 mM EHAC micellar solutions at NaCl concentrations of 60 mM (△), 100 mM (□), 600 mM (■), 800 mM (○), and 1000 mM (●). The sample viscosity is normalized by its zero-shear value and plotted versus the Weissenberg number $Wi \equiv \dot{\gamma}\tau_R$.

in Figure 2b for these samples correspond to a shear rate of 10^{-4} s^{-1}. Beyond the maximum, the viscosity drops until the point of phase separation. All solutions investigated show steady-shear rheological behavior typical of entangled wormlike micelles, as seen in Figure 3 where the viscosity, normalized by its zero-shear value η_0, is plotted as a function of the Weissenberg number $Wi \equiv \dot{\gamma}\tau_R$ for selected EHAC/NaCl samples. The relaxation time τ_R is the inverse of the critical shear rate at which the viscosity begins to decrease. In all cases, the rheology shows a Newtonian viscosity plateau at low shear rates ($Wi < 1$), followed by rapid shear thinning at high shear rates ($Wi > 1$).

Solutions with high salt content became noticeably turbid on shearing. This was observed visually in many cases, e.g., for a 40 mM EHAC + 1000 mM NaCl sample. Initially, the solution was clear and bluish, but when the vial was shaken lightly, parts of the sample turned cloudy and further shaking resulted in an entirely turbid sample. Upon cessation of shear, the turbidity persisted for a few minutes before gradually clearing. These simple visual observations suggested that the sample undergoes a reversible, shear-induced phase separation. The micellar solutions exhibiting this effect (marked in Figure 2b with filled circles) all have higher salt concentrations than that at the viscosity maximum. Micellar solutions at NaCl concentrations less than about 200 mM showed no visible signs of turbidity upon shaking.

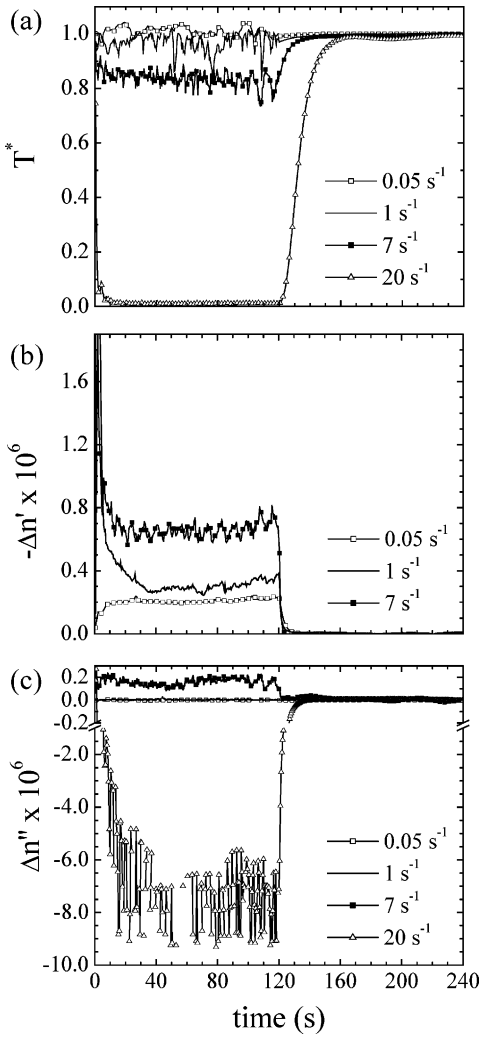

Figure 4. Transient rheo-optic experiments on a 40 mM EHAC + 1000 mM NaCl sample in H_2O. The normalized transmittance T^* (a), the flow-birefringence $\Delta n'$ (b), and the flow-dichroism $\Delta n''$ (c) are shown as a function of time during and after shear rates of 0.05, 1, 7, and 20 s^{-1}. The shear zone is 120 s and is followed by 120 s of relaxation.

Rheo-Optic Studies. Rheo-optic measurements were performed at 25 °C on 40 mM EHAC micellar solutions at several NaCl concentrations to investigate the shear-induced turbidity and to determine if there is anisotropy in the structure. The time-dependent development of turbidity, dichroism, and birefringence during shear and their disappearance after cessation of shear are shown in Figure 4 for a 40 mM EHAC + 1000 mM NaCl sample. Here, the normalized transmittance T^*, birefringence $\Delta n'$, and dichroism $\Delta n''$ are plotted as a function of time for shear rates in the Newtonian and shear-thinning regimes. The transmittance T^* (Figure 4a) is equal to 1 (clear sample) during shear rates of 0.05 and 1 s^{-1} but decreases to 0.84 when the shear rate is increased to 7 s^{-1}. In the latter case, T^* relaxes to a value of 1 within 30 s after

shear is stopped. The solution is completely turbid ($T^* \rightarrow 0$) at a shear rate of 20 s^{-1} but regains clarity within 40 s after shear cessation.

The measured birefringence during this transition is shown in Figure 4b. At a low shear rate of 0.05 s^{-1} ($Wi = 0.4$), $\Delta n'$ quickly reaches a steady-state value of -0.2×10^{-6}. Upon cessation of shear, $\Delta n'$ quickly relaxes to zero (within 10 s), indicating that the micellar solution quickly reverts to an isotropic state. At a higher shear rate of 1 s^{-1} ($Wi = 7$), $\Delta n'$ initially goes through a sharp overshoot and thereafter reaches a steady value of $-0.3 \pm 0.05 \times 10^{-6}$. The birefringence continues to increase with shear rate, and at shear rates of 20 s^{-1} or higher, its value exceeds the instrument resolution ($\sim 8 \times 10^{-6}$). The birefringence is presumably due to micellar segmental alignment in the flow direction, and its negative value is a consequence of the negative intrinsic birefringence of the micelle segments.[29] Typically, the higher the shear rate, the greater the flow-induced alignment. As the extra stress is primarily due to chain stretch, a stress-optic relationship between the flow-birefringence and the shear stress is expected:[32]

$$\Delta n' \sin 2\chi = 2C\sigma \tag{4}$$

Here χ is the orientation angle of the micelles relative to the flow and C is the stress-optic coefficient. As expected,[32] χ drops from a value of 45° at rest to a low value ($\sim 5°$) at high shear rates, indicating alignment of micelle segments with the flow direction (data not shown).

Finally, the flow-dichroism measurements, which reflect the anisotropy of any flow-induced structures, are shown in Figure 4c. At shear rates of 0.05 and 1 s^{-1}, where T^* remains equal to 1, no dichroism is detected. At a higher rate well into the shear-thinning regime (7 s^{-1}, $Wi = 50$), the solution also shows a small, positive dichroism ($\Delta n'' \approx 0.2 \times 10^{-7}$), which relaxes back to zero after shear is stopped. For a shear rate of 20 s^{-1}, the dichroism is negative and larger in magnitude (ca. -7.7×10^{-6}), but the signal is very noisy due to the small value of T^*.

The steady-state values of T^*, $\Delta n'$, and $\Delta n''$ are shown as a function of Weissenberg number for the 40 mM EHAC + 1000 mM NaCl sample in Figure 5a. The birefringence becomes nonzero at $Wi < 1$ and continues to increase with shear rate. The dichroism only becomes nonzero at $Wi \approx 50$, corresponding to the decrease of T^*. Figure 5b shows the steady-state values of T^* and $\Delta n''$ for a sample of 40 mM EHAC + 60 mM NaCl, which has a comparable zero-shear viscosity (Table 1). In this case, no measurable turbidity or dichroism is observed over a similar range of Wi, in accordance with visual observations.

Rheo-optic experiments were performed for solutions at various NaCl concentrations. To quantitatively compare the data, the loss of transmittance with increasing shear rate was fit to the empirical form

$$T^*(\dot\gamma) = \frac{1}{[1 + (\dot\gamma/\dot\gamma_m)^p]} \tag{5}$$

where $\dot\gamma_m$ is the shear rate at which T^* equals 0.5, and p is related to the rate of decay of T^* with shear rate. Table 1 shows the fitted parameters for 40 mM EHAC solutions with NaCl concentrations of 600, 800, and 1000 mM. As the salt concentration increases (and thereby, the phase boundary is approached), the shear rate $\dot\gamma_m$ increases and T^* decays more rapidly. The presence of elastic instabilities

(32) Shikata, T.; Dahman, S. J.; Pearson, D. S. *Langmuir* **1994**, *10*, 3470−3476.

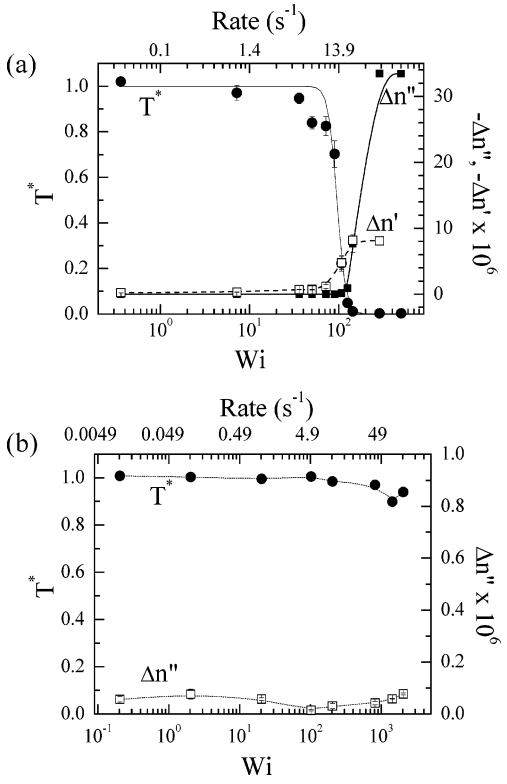

Figure 5. (a) Steady-state values of T^* (●), $\Delta n'$ (□), and $\Delta n''$ (■) as a function of Weissenberg number Wi for a 40 mM EHAC + 1000 mM NaCl micellar solution. (b) Steady-state values of T^* (●) and $\Delta n''$ (□) as a function of Wi for 40 mM EHAC + 60 mM NaCl. The corresponding shear rates are shown for reference on each plot.

Table 1. Parameters from the Empirical Fit to T^* versus Shear Rate Data for 40 mM EHAC Solutions with Various NaCl Concentrations

salt	c_{salt} (mM)	η_0 (Pa s)	τ_R (s)	$\dot\gamma_m$ (s^{-1})	p	$Wi_m = \dot\gamma_m \tau_R$
NaCl	60	12.8	13.2	n/a	n/a	n/a
NaCl	100	820	166	n/a	n/a	n/a
NaCl	600	137	47.5	1.1 ± 0.1	2.1 ± 0.2	54 ± 3
NaCl	800	44.9	10.8	3.9 ± 0.1	4.9 ± 0.8	66 ± 2
NaCl	1000	24.2	7.2	13.3 ± 0.3	9.1 ± 1.8	110 ± 3

(rod-climbing) in the 40 mM EHAC + 400 mM NaCl sample made it difficult to quantify rheo-optic data for this case; however, $\dot\gamma_m$ was roughly in the range 0.04−0.2 s^{-1}, consistent with the above trends. No shear-induced turbidity was detected for $c_{NaCl} = 60$, 100, and 200 mM.

To our knowledge, there are no previous reports of flow-dichroism in wormlike micellar solutions. Note that dichroism refers to the complex part of the refractive index tensor and it can arise due to anisotropy in either light absorption or scattering.[6] Because typical wormlike micellar solutions are optically clear, there is little reason to expect them to be dichroic, either at rest or under flow. On the other hand, flow-dichroism does occur in polymer solutions exhibiting shear-induced phase separation[6] due to scattering from concentration fluctuations oriented by the flow. In the micellar systems under consideration here, a similar scattering of light by flow-induced structures in solution must be responsible for the flow-dichroism. These structures must be several microns or larger, judging from the visual appearance of turbidity, and we therefore attempted to detect their presence using scattering techniques.

Flow-SANS Studies. Flow-SANS experiments were performed on EHAC/NaCl micelles, with D_2O as the

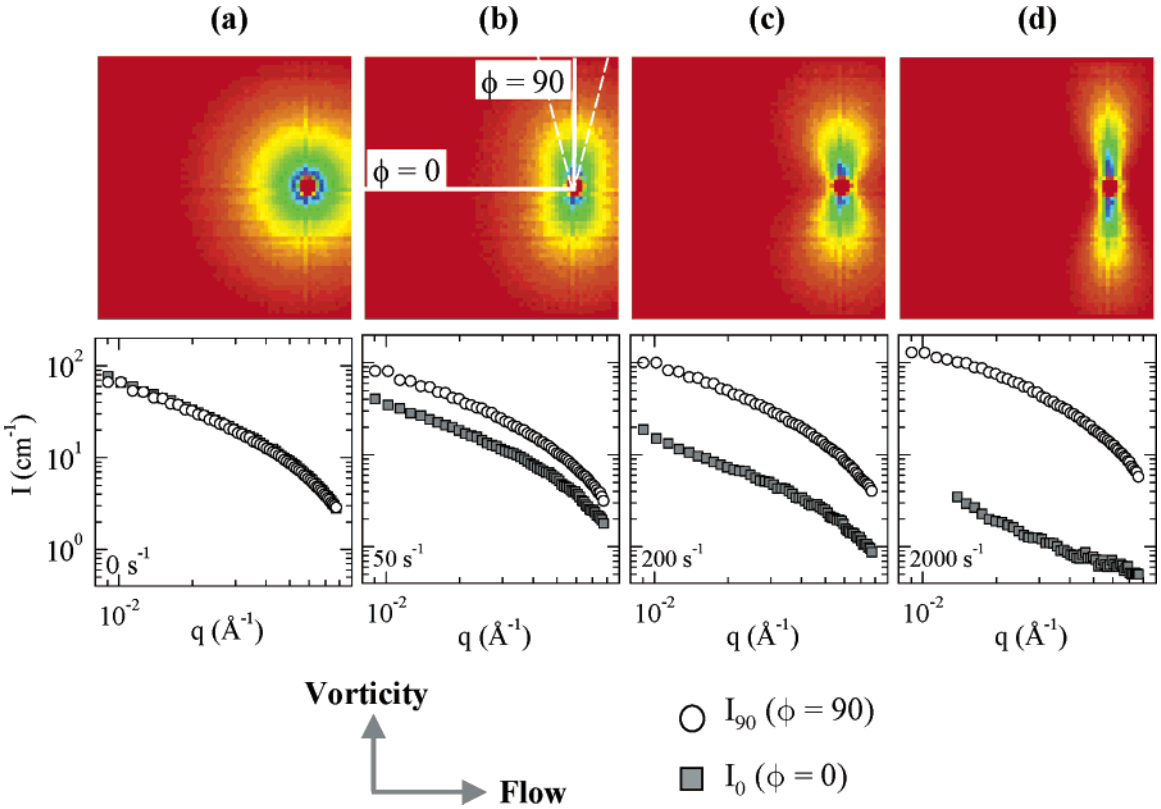

Figure 6. 2D flow-SANS patterns at different shear rates for a sample of 40 mM EHAC + 900 mM NaCl in D_2O. The plots below show the sector-averaged intensity I about the flow (I_0) and vorticity (I_{90}) directions extracted from the 2D patterns.

solvent. The phase diagram of EHAC + NaCl in D_2O is slightly shifted relative to that in H_2O such that a composition of 40 mM EHAC + 1000 mM NaCl in D_2O is now in the two-phase region. Reducing the salt concentration to 900 mM resulted in a single-phase sample whose rheology and phase behavior closely mimicked that of the H_2O fluid studied earlier. This D_2O solution also turned visibly turbid upon shearing, and the turbidity disappeared gradually once the shear was stopped.

Two-dimensional SANS patterns were collected at rest and under shear at shear rates spanning the Newtonian and shear-thinning regimes. Representative patterns (flow direction horizontal, vorticity direction vertical) are shown in Figure 6 for the 40 mM EHAC + 900 mM NaCl sample. The rest pattern is isotropic in the flow-vorticity plane, indicating no preferred orientation of the micelles. The pattern continues to remain isotropic at low shear rates ($<10\ s^{-1}$). At a shear rate of $50\ s^{-1}$, the pattern is noticeably elongated in the vorticity direction. With further increases in shear rate, the pattern elongates further, assuming a two-lobed shape at $200\ s^{-1}$ and a needlelike shape at $2000\ s^{-1}$. The increase in scattered intensity I in the vorticity direction and its corresponding decrease in the flow direction are shown in the accompanying sector-average I versus q plots (15° sectors). These trends are consistent with the shear-induced alignment of wormlike chains.[33] The shapes of the I versus q plots remain virtually identical over the entire shear-rate range, which suggests that the wormlike chains align under flow without any significant molecular rearrangement on the length scales probed by SANS.

The alignment factor A_f (eq 4) is shown as a function of shear rate and Weissenberg number in Figure 7 for the 40 mM EHAC + 900 mM NaCl sample. Micellar alignment

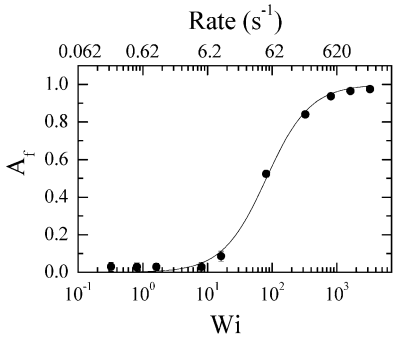

Figure 7. Alignment factor based on the flow-SANS sector-averaged data (see text) for the 40 mM EHAC + 900 mM NaCl sample in D_2O as a function of the Weissenberg number. The line is a fit to the data using eq 6.

becomes evident at $Wi > 10$, and the micelles are almost completely aligned at $Wi > 1000$. To compare the micellar alignment in various samples, the alignment factor data are fit to the following form:

$$A_f(\dot{\gamma}) = 1 - \frac{1}{1 + (\dot{\gamma}/\dot{\gamma}_{m,SANS})^p} \qquad (6)$$

where $\dot{\gamma}_{m,SANS}$ is the shear rate at which $A_f = 0.5$, and p is related to the rate of increase of A_f with shear rate. The fitted parameters are shown in Table 2 for various NaCl concentrations. The critical shear rate shows a minimum at 200 mM NaCl, the location of the maximum in viscosity and relaxation time, while the critical Weissenberg number (where $A_f = 0.5$) decreases with increasing NaCl concentration. There is negligible evidence of alignment (i.e., $A_f \approx 0$) until relatively large Wi, whereupon A_f rises steeply. Note that in the case of rheo-optic experiments, which were done in the flow-gradient plane, birefringence

(33) Penfold, J.; Staples, E.; Cummins, P. G. *Adv. Colloid Interface Sci.* **1991**, *34*, 451.

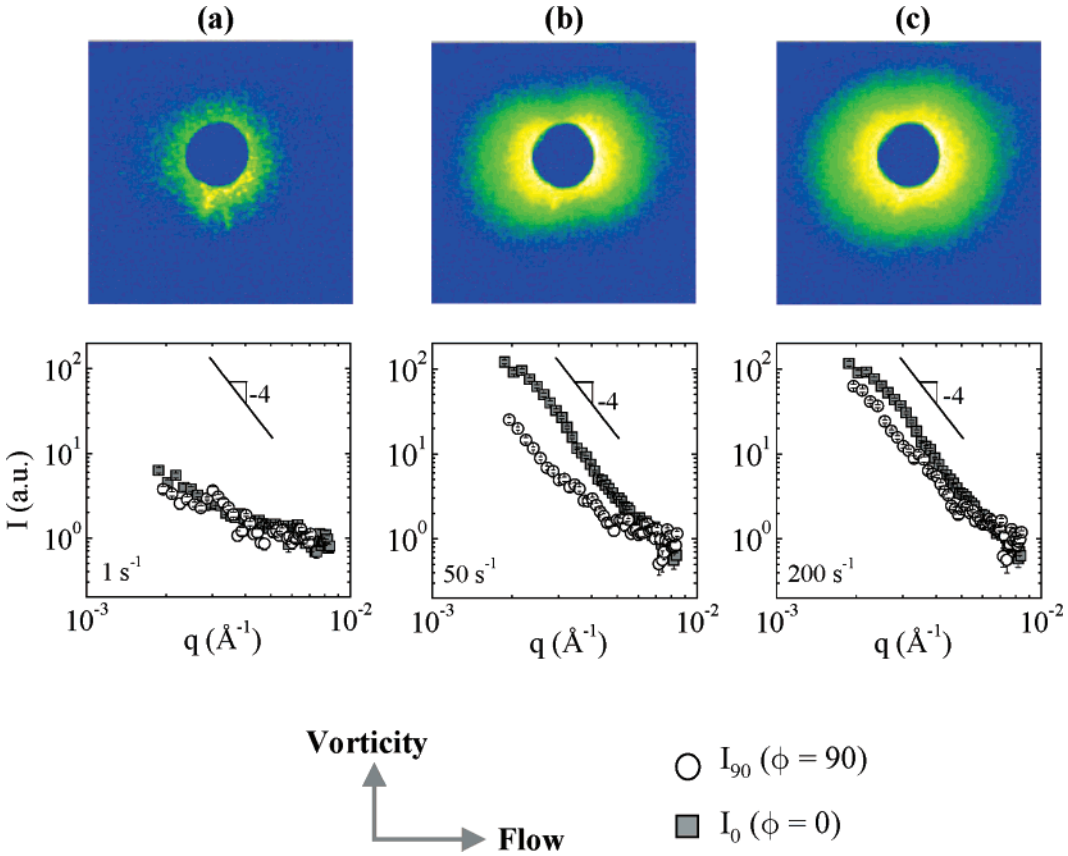

Figure 8. 2D flow-SALS patterns for a sample of 40 mM EHAC + 1000 mM NaCl in H_2O at shear rates of (a) 1 s^{-1}, (b) 50 s^{-1}, and (c) 200 s^{-1}. The plots below show the sector-averaged intensity I about the flow (I_0) and vorticity (I_{90}) directions extracted from the 2D patterns.

Table 2. Parameters from the Empirical Fit to Shear-SANS Data for 40 mM EHAC Solutions with Various Salt Concentrations

salt	c_{salt} (mM)	$\dot{\gamma}_{m,SANS}$ (s^{-1})	p	$Wi_{m,SANS}$
NaCl	55	215 ± 21	0.59 ± 0.04	25000 ± 2000
NaCl	200	3.4 ± 1.3	0.34 ± 0.05	3400 ± 1300
NaCl	600	14.5 ± 0.9	1.01 ± 0.06	490 ± 30
NaCl	875	71 ± 8	0.98 ± 0.1	425 ± 50
NaCl	900	50 ± 34	1.3 ± 0.1	81 ± 6

and hence segmental alignment were observed at much lower shear rates.

Flow-SALS Studies. There is no increase in the low-q scattering of neutrons from samples under shear, implying that any shear-induced structures formed are too large to fall within the range of scattering vectors probed by SANS. Therefore, we performed flow-SALS experiments on selected samples (identical to those studied by rheo-optics). Figure 8 shows two-dimensional SALS patterns from a 40 mM EHAC + 1000 mM NaCl micellar solution for shear rates of 1, 50, and 200 s^{-1}, with corresponding sector averages of the intensity in the flow (I_0, $\phi = 0$) and vorticity (I_{90}, $\phi = 90$) directions. The scattered intensity at $\dot{\gamma} = 1$ s^{-1} remains isotropic (Figure 8a), with I_0 and I_{90} overlapping at all q. There is little to no increase in the scattered intensity at 1 s^{-1} compared to the rest state, even though the solution is birefringent (Figure 4) and within the shear-thinning regime (Figure 3) at this shear rate. At $\dot{\gamma} = 50$ s^{-1} ($Wi = 360$), the scattering in the flow direction is enhanced and a "butterfly" pattern is evident. The slope of I_0 versus q approaches −4, indicating the presence of sharp interfaces, possibly phase-separated domains.[34] As the shear rate is further increased to 200 s^{-1} ($Wi = 1400$), the scattering pattern becomes more isotropic, with I_{90} also showing the q^{-4} scaling.

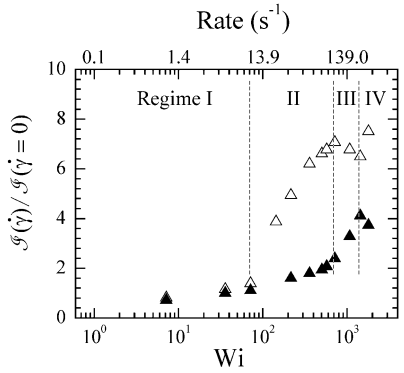

Figure 9. Integrated flow-SALS intensities along the flow $\mathcal{J}_x$ (△) and vorticity $\mathcal{J}_z$ (▲) directions as a function of Weissenberg number for the 40 mM EHAC + 1000 mM NaCl sample.

Figure 9 shows the integrated intensities (eqs 1 and 2) along the flow ($\mathcal{J}_x$) and vorticity ($\mathcal{J}_z$) directions as a function of shear rate and Wi for the 40 mM EHAC + 1000 mM NaCl sample. At low shear rates, the scattering under shear is identical to the scattering at rest (regime I). At about 10 s^{-1} ($Wi \approx 70$), the scattering in the flow direction $\mathcal{J}_x$ begins to increase, while that in the vorticity direction $\mathcal{J}_z$ remains unchanged (regime II). This shear rate correlates with the onset of strong turbidity in rheo-optics (Table 1). As the shear rate is increased to 50 s^{-1}, $\mathcal{J}_x$ saturates, while $\mathcal{J}_z$ begins to rise (regime III). Finally, above a shear rate of 150 s^{-1}, $\mathcal{J}_x$ and $\mathcal{J}_z$ show anomalous oscillations (regime IV). Data for 40 mM EHAC solutions with 600 and 800 mM NaCl show the same qualitative

(34) Porod, G. *Kolloid Z. Z. Polym.* **1951**, *124*, 83.

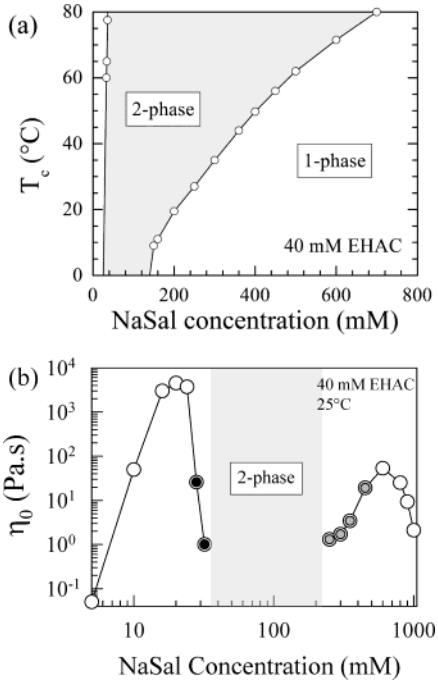

Figure 10. Phase behavior and rheology of EHAC/NaSal mixtures at a fixed EHAC content of 40 mM (ref 28): (a) coexistence temperature T_c vs salt concentration; (b) zero-shear viscosity η_0 at 25 °C vs salt concentration. The filled circles in panel (b) denote samples that show shear-induced turbidity.

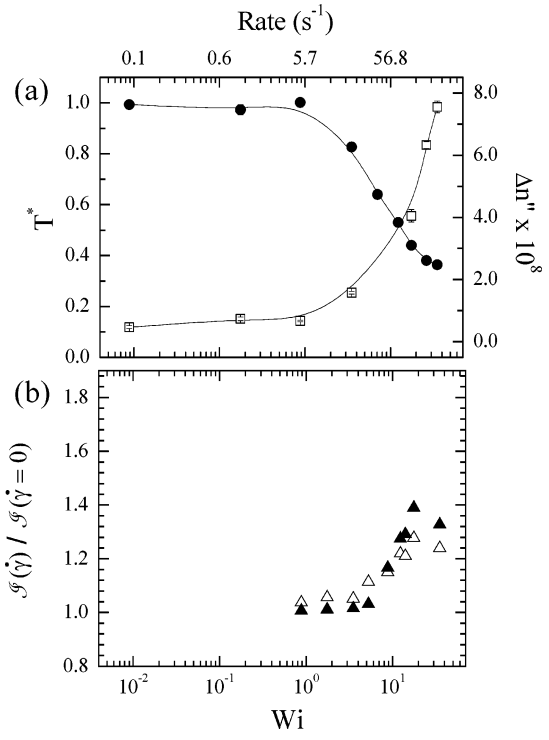

Figure 11. Rheo-optic and flow-SALS experiments on a 40 mM EHAC + 250 mM NaSal sample. (a) Steady-state values of T^* (●) and $\Delta n''$ (□) as a function of the Weissenberg number. (b) Integrated flow-SALS intensities along the flow $\mathcal{J}_x$ (△) and vorticity $\mathcal{J}_z$ (▲) directions as a function of the Weissenberg number.

behavior, with the transition shear rates at the onset of regime II being ca. 0.1 and 2 s^{-1}, respectively, which are also in good agreement with the onset of turbidity from rheo-optic experiments. As discussed presently, the above trends in flow-SALS for wormlike micellar solutions undergoing SIPS are similar to those observed for polymer solutions during SIPS.

B. EHAC/Sodium Salicylate (NaSal) Micellar Solutions. Shear-induced turbidity also occurs in solutions of EHAC with other simple salts, including potassium chloride (KCl) and calcium chloride ($CaCl_2$), where it is observed at high salt content, just as with NaCl solutions. In addition, hydrotropic salts such as sodium salicylate (NaSal) can induce EHAC to form wormlike micelles at much lower salt concentrations, and some EHAC/NaSal solutions also show shear-induced turbidity. The phase behavior of the EHAC/NaSal system at 40 mM EHAC is reproduced in Figure 10a.[28] The first of the two phase boundaries, appearing at low salt concentrations (c_{NaSal} = 30−40 mM), is of the upper consolute type, that is, the samples separate into two phases upon cooling. Subsequently, for c_{NaSal} of 150 mM or higher, there is a lower consolute phase boundary, that is, the samples turn cloudy when heated above the coexistence curve. The coexistence or cloud point temperature monotonically increases with increasing c_{NaSal}.

The rheology of EHAC/NaSal solutions[27,28] at 25 °C is reproduced in Figure 10b. In this case, the zero-shear viscosity η_0 shows two maxima as a function of c_{NaSal}. Samples near the first viscosity maximum are gels, as was noted in the case of EHAC/NaCl, and the viscosity values shown for the gels correspond to a shear rate of 10^{-4} s^{-1}. Beyond the first maximum, the viscosity drops till the phase boundary is reached. Subsequently, there is another viscosity maximum at about 600 mM NaSal in the second single-phase region.

Shear-induced turbidity is visually observed in the EHAC/NaSal samples marked with filled circles on the viscosity plot (Figure 10b). Visual observations reveal a significant difference between the turbidity in the low- and high-salt samples. In the low-salt samples, which fall on the descending side of the first viscosity curve (black symbols in Figure 10b), the turbidity is pronounced and long-lived, persisting for several hours or even days before the sample returns to a single-phase state. In the case of the high-salt samples located on the ascending side of the second curve (gray symbols), the turbidity is weak; it appears only upon a more intense shaking of the vial, and the sample returns to a clear state almost immediately upon stopping shear.

To quantify these differences, rheo-optic and flow-SALS experiments were performed on EHAC/NaSal samples along each branch of the viscosity plot. Rheo-optic experiments on a 40 mM EHAC + 250 mM NaSal solution show a gradual drop in T^* as the shear rate is increased (Figure 11a), with the solution never becoming completely turbid. Over the shear rates examined, the dichroism remains positive, with its value about 2 orders of magnitude less than for the NaCl samples. Flow-SALS experiments on this sample do not show butterfly patterns, although an increase in intensity is observed at high shear rates (Figure 11b). The integrated intensities along the flow $\mathcal{J}_x$ and vorticity $\mathcal{J}_z$ directions both increase in accord at $Wi \sim 4$, such that the 2D scattering pattern remains isotropic. The increase in scattered intensity under shear is also considerably less than that for the EHAC/NaCl solutions, and the −4 slope of I versus q is not observed (data not shown). In the case of a 40 mM EHAC + 30 mM NaSal solution, the rheo-optic data were difficult to reproduce and are not shown. However, the experiments confirmed the visual observations in that T^* dropped to a low value at shear rates around 1 s^{-1} and did not recover over the time period studied. Inspection of the sample following

the experiment confirmed that it remained turbid and inhomogeneous.

Discussion

We have demonstrated shear-induced phase separation (SIPS) in EHAC micellar solutions containing either NaCl at concentrations of ≥400 mM or NaSal at concentrations of 24−32 or 250−400 mM. The SIPS manifests as a reversible turbidity, which is observed upon gentle shaking of a vial, and verified quantitatively through rheo-optic experiments that measure the transmittance of light under shear. The onset of turbidity occurs when the shear rate exceeds a critical value, and this coincides with the development of a finite dichroism in the micellar sample. On the other hand, both clear and turbid micellar solutions show flow-birefringence as well as anisotropic flow-SANS patterns, which are both indicative of segmental alignment along the flow direction (Figure 7, Table 2). Thus it is the flow-dichroism that correlates with the turbidity, and both effects may be attributed to scattering from large, phase-separated domains. These domains are typically oriented along the vorticity direction, leading to the negative dichroism and the butterfly patterns in flow-SALS experiments.[6,8]

The above observations of SIPS in wormlike micellar solutions are quite analogous to those for SIPS in polymer solutions, suggesting that similar mechanisms are operative in both cases. In polymer solutions, the SIPS results have been classified into four regimes.[35] In regime I, typically corresponding to a pseudo-Newtonian viscosity, no turbidity is observed and the solution is birefringent but not dichroic. Scattering patterns are isotropic, and there is no increase in scattered intensity relative to the quiescent state. Above a transition shear rate $\dot{\gamma}_c$ (regime II), the solution becomes turbid with a small, negative dichroism, and a butterfly pattern is seen in flow-SALS and/or SANS experiments. Consistent with these results, micron-sized, elongated domains oriented along the vorticity direction are observed in shear-microscopy images.[8] With increasing shear rate in regime II, the scattered intensity in the flow direction $\mathcal{J}_x$ increases, causing the butterfly "wings" to enlarge. As the shear rate is increased further, $\mathcal{J}_x$ eventually reaches a plateau (regime III).[11,31,35] This saturation in $\mathcal{J}_x$ is accompanied by an increase in $\mathcal{J}_z$, the scattering in the vorticity direction, causing the butterfly pattern to become more isotropic. An anomalous regime (regime IV) may be present above a second critical rate $\dot{\gamma}_a$, in which the dichroism and birefringence are very large, and the dichroism undergoes a sign reversal from negative to positive.[11,31,35] The integrated SALS intensities may plateau or oscillate with increasing shear rate.[11,31,35] A streaklike pattern with intense scattering in the vorticity direction may also be found in regime IV, where shear microscopy shows a stringlike phase oriented along the flow.

In the EHAC/NaCl solutions that show SIPS, all the above regimes are evident (Figure 9). At low shear rates (regime I) within the Newtonian plateau and the beginning of the shear-thinning region, only birefringence is observed due to segmental alignment. Above a transition shear rate (regime II), the solution becomes turbid with a negative dichroism, and correspondingly, flow-SALS shows butterfly patterns, with the butterfly "wings" enlarging with increasing shear rate. These features are all consistent with the growth of concentration fluctuations oriented along the vorticity axis. The integrated SALS intensity in the flow direction $\mathcal{J}_x$ continues to increase in this regime. As $\mathcal{J}_x$ saturates, the intensity in the vorticity direction $\mathcal{J}_z$ increases (regime III). Finally, in regime IV, both $\mathcal{J}_x$ and $\mathcal{J}_z$ show anomalous oscillations.

The EHAC/NaSal micellar solutions exhibit several differences from the EHAC/NaCl solutions with regard to their SIPS behavior. On one hand, the low NaSal (30 mM) sample shows a long-lived SIPS, with the turbidity taking hours to days to recover back to the quiescent state (much longer than the rheological relaxation time). In contrast, the 250 mM NaSal sample, which is close to a lower consolute phase boundary, shows only a weak SIPS. Both the turbidity and the dichroism are significantly weaker than in the NaCl solutions, that is, $\Delta n''$ does not saturate, nor does T^* reach zero (Figure 11a). Flow-SALS shows only a moderate increase in scattering in the flow and vorticity directions, both increasing in tandem at the same critical shear rate and thereby leading to an isotropic scattering pattern rather than the signature butterfly pattern. These results suggest a more isotropic growth of concentration fluctuations due to shear in this sample.

In polymer solutions, the critical shear rate for SIPS (onset of regime II) often corresponds to the onset of shear thinning ($Wi_c \equiv \dot{\gamma}_c\tau \approx 1$). In turn, $\dot{\gamma}_c$ depends on the thermodynamic and viscoelastic material properties, such as temperature or polymer concentration.[31] The Helfand−Fredrickson (HF) linear theory[5] predicts $\dot{\gamma}_c \approx K_{os}/5\eta_0$, where K_{os} is the osmotic modulus. In the case of EHAC/NaCl micellar solutions, the critical shear rate for SIPS increases with NaCl concentration over the range $400 \leq c_{NaCl} \leq 1000$ mM. Since the zero-shear viscosity decreases with c_{NaCl} over this range (Table 1), the observed trend for $\dot{\gamma}_c$ is consistent with the HF prediction.

In contrast to polymer solutions, however, the onset of SIPS in EHAC micellar solutions occurs at Weissenberg numbers $Wi_c \sim 10$ or larger. That is, in all samples showing SIPS, the shear rate required to induce turbidity is larger than that which results in the onset of shear thinning. Presumably, this means that a greater shear stress is required to orient the concentration fluctuations in micellar solutions compared to polymer solutions. The above finding additionally shows that the phase separation discussed here does not correspond to the formation of shear bands[17] or an isotropic-to-nematic phase transition,[18] that is, to phenomena related to the onset of shear thinning. Furthermore, the shear-induced turbidity and dichroism are not characteristic of all entangled wormlike micellar solutions but are only manifested in EHAC micellar samples over certain salt concentrations.

As discussed, the similarity in SIPS behavior of polymers and micelles strongly implicates the role of critical concentration fluctuations, with the turbidity being caused by the coupling of shear stress to these fluctuations.[36,37] Indeed, micellar solutions that showed SIPS also exhibited an opalescent bluish color, which is indicative of scattering from concentration fluctuations with sizes on the order of the wavelength of light. The bluish tinge became stronger on approaching the temperature−salt phase boundaries in Figures 2 and 10, indicating growth of these fluctuations, and it is probably no coincidence that the SIPS became stronger near the same phase boundaries as well. In contrast, samples farther away from the phase boundaries were practically colorless and did not show SIPS.

The above observations emphasize the close link between the equilibrium and nonequilibrium (shear-induced) phase behavior in the micellar fluids studied.

(35) Hashimoto, T.; Kume, T. *J. Phys. Soc. Jpn.* **1992**, *61*, 1839.

(36) Schmitt, V.; Marques, C. M.; Lequeux, F. *Phys. Rev. E* **1995**, *52*, 4009.

(37) Olmsted, P. D.; Lu, C. Y. D. *Phys. Rev. E* **1997**, *56*, R55.

Previous reports of shear-induced turbidity in wormlike micellar solutions[16−25] were not placed in the context of the underlying equilibrium phase behavior. However, it is interesting that the systems studied by Pine et al.[19−22] and Fischer et al.[21,22] both contained equimolar concentrations of cationic surfactant and NaSal. In our case, an equimolar mixture of EHAC and NaSal falls within the two-phase region of the phase diagram (Figure 9a), while a sample close to the equimolar ratio (Figure 10a) shows strong shear-induced turbidity. Therefore, it is plausible that the previous observations of shear-induced turbidity are also a consequence of concentration fluctuations and their shear-induced growth in the respective samples.

While the importance of the equilibrium phase behavior is evident, the solution microstructure also may play a role in the present context. In contrast to polymers, the length, flexibility, and structure of micelles may be altered as a phase boundary is approached. Earlier, we had postulated a transition from linear to branched micelles to explain the rheology and phase behavior of EHAC micellar systems as a function of salt.[28] According to this hypothesis, samples close to the phase boundaries in Figures 2 and 10 (which correspond to the decreasing portion of viscosity curves) contain a substantial amount of branched wormlike micelles. This hypothesis is relevant here, since the *same samples* also show shear-induced turbidity.

A sensible scenario that can tie together these findings is that linear micelles transform into branched micelles as the solvent environment around them deteriorates. Note that in the case of polymers, the θ-point corresponds to the limit of marginal solvency, and shear-induced phase separation occurs near the θ-point. A similar limit of marginal solvency may well exist for micelles in water. Adding salt may reduce the "solvent quality" of water for the micelles, causing the micelles to branch. As branching progresses, the micelles are expected to form a bicontinuous "cross-linked" network, and the system eventually phase-separates when the associated entropic penalty becomes too high.[38,39] Thus the branching of micelles near a phase boundary can be qualitatively compared to the shrinking of polymer coils near the θ-point. Indeed, the presence of highly branched or "bicontinuous" micelles may even be a necessary criterion for shear-induced phase separation to occur in micellar fluids. The recent observation of the same phenomenon in a bicontinuous microemulsion[15] supports this notion.

Conclusions

We have presented observations of shear-induced phase separation in solutions of wormlike micelles. The phenomenon occurs for solutions in which long-ranged concentration fluctuations are present. Rheo-optic studies show that the effect of shear is to enhance and orient these fluctuations, leading to a nonzero dichroism signal under shear. The oriented domains typically lie along the vorticity axis, leading to a butterfly pattern in flow-SALS, with enhanced scattering in the flow direction and a concomitant depression of scattering along the vorticity direction. The domains are too large to be detected by flow-SANS, however.

While the underlying physics for shear-induced phase separation in both polymeric and wormlike micellar systems may be similar, there are important differences as well. In the case of polymers, the polymer coils contract as the θ-point (limit of poor solvency) is approached. In micellar systems, the deteriorating "solvent quality" may drive a transition from linear to branched micelles. The eventual formation of a bicontinuous or "cross-linked" network of highly branched micelles may denote the limit of poor solvency, and we expect shear-induced phase separation to occur in samples close to this limit.

Acknowledgments. We acknowledge NIST for facilitating the flow-SANS experiments performed as part of this work. S.R.R. also acknowledges helpful discussions with Professor Wesley Burghardt (Northwestern University) and Dr. Jack Douglas (Polymers Division, NIST).

LA035810D

(38) Cristobal, G.; Rouch, J.; Curely, J.; Panizza, P. *Physica A* **1999**, *268*, 50.

(39) Bernheim-Groswasser, A.; Wachtel, E.; Talmon, Y. *Langmuir* **2000**, *16*, 4131.